Macromolecules

Article

Cite This: Macromolecules 2019, 52, 6055−6067

pubs.acs.org/Macromolecules

Manipulating the Mechanical Response of Hydrophobically Cross-Linked Hydrogels with Ionic Associations

Chao Wang,[†,§] Katherine Deitrick,[†,∥] Junyoung Seo,[†] Ziwei Cheng,[‡] Nicole S. Zacharia,[†] R. A. Weiss,*[,†] and Bryan D. Vogt*[,†]

[†]Department of Polymer Engineering, University of Akron, 250 South Forge Street, Akron, Ohio 44325, United States

[‡]Department of Chemical and Biomolecular Engineering, Catalysis Center for Energy Innovation, University of Delaware, 221 Academy Street, Newark, Delaware 19716, United States

Supporting Information

ABSTRACT: To prevent brittle failure, tough hydrogels rely on energy dissipation, which can be manifested through sacrificial covalent bonds or reversible, noncovalent cross-links. However, these noncovalent cross-links tend to lead to significant creep during deformation due to rearrangements of the effective cross-links. Here, the influence of ionic associations as a secondary network in noncovalently cross-linked hydrogels is examined using a terpolymer of hydroxyethyl acrylate (HEA), 2-(*N*-ethylperfluorooctanesulfonamido)ethyl methacrylate (FOSM), and zinc diacrylate (ZnA). Despite the solubility of HEA−ZnA copolymers in water, the incorporation of ionic moieties that contain stoichiometric quantities of zinc into a network cross-linked by hydrophobic associations significantly increased the effective cross-link density. The terpolymer-based hydrogel contained ≈90% of the water of a HEA−FOSM copolymer hydrogel with the same FOSM content, but the storage modulus was nearly an order of magnitude larger than for the terpolymer hydrogel. To obtain the same storage modulus, the FOSM content for the copolymer hydrogel would need to be more than doubled, but this hydrogel has almost 40% less water than the terpolymer hydrogel. The terpolymer-based hydrogel exhibited improved creep resistance by increasing the relaxation times through the synergistic effect of hydrophobic and ionic associations. On recovery from creep, the terpolymer-based hydrogel responded primarily elastically. Despite this elastic-like behavior, the terpolymer-based hydrogel can also efficiently self-heal its microstructure. These results illustrate the ability to dramatically alter the mechanical response of hydrogels through ionic associations even when only stoichiometric quantities of Zn^{2+} are present.

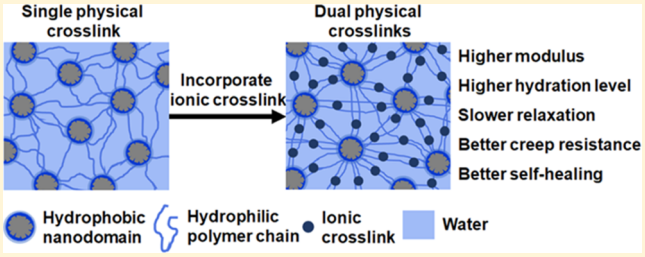

INTRODUCTION

Tough hydrogels hold significant promise for numerous biomedical applications as their mechanical properties can mimic those of natural tissue.[1−4] In general, hydrogels are elastic solids and when swollen to equilibrium, the network chains are highly extended. As a result, hydrogels are usually brittle, since there are no viscous mechanisms to relieve stress and the swollen chains have finite extensibility. To impart toughness to a hydrogel, energy dissipation mechanisms must be introduced. One approach for developing tough hydrogels is the double-network (DN) hydrogels that were first discovered by Gong et al.[5] For those materials, breaking of sacrificial covalent bonds provides energy dissipation.[6] However, this results in irreversible, permanent damage of the cross-linked network that produces poor fatigue resistance and deterioration of the mechanical performance of the DN hydrogel upon cyclic loading.[7] An alternative approach for toughening hydrogels is to employ noncovalent, supramolecular cross-links such as hydrogen bonds,[8−10] ionic bonds,[11−14] or hydrophobic associations[15−18] that provide a reversible energy dissipation mechanism, in that physical cross-links can break to relieve the applied stress but then reform after the stress is dissipated. The reversibility of the supramolecular cross-links also produces a route for self-healing of the hydrogel after deformation.[14] In principle, one wishes that the bonds between specific functional groups reform to preserve exactly the same chain conformations that existed before the reversible bonds were broken, but in practice, the physical bonds may reform between different functional groups, which rearranges the conformations of the network chains. In that case, some permanent, plastic deformation occurs and the hydrogel properties change, though not to the same extent as occurs when the network is irreversibly broken. The viscoelastic nature of the cross-linked network also produces creep deformation of the hydrogel when a load is applied.[19,20] Creep is a viscous phenomenon and can be minimized by maximizing the elastic character of the supramolecular hydrogel. However, increasing the elastic character can have detrimental effects on the toughness. So, the challenge with designing supramolecular, tough hydrogels is to control the

Received: April 22, 2019
Revised: July 22, 2019
Published: August 5, 2019

Downloaded via UNIV OF AKRON on March 31, 2020 at 21:05:52 (UTC).
See https://pubs.acs.org/sharingguidelines for options on how to legitimately share published articles.

© 2019 American Chemical Society

DOI: 10.1021/acs.macromol.9b00830
Macromolecules 2019, 52, 6055−6067

strength of the supramolecular bonds such that they are sufficiently weak to provide a suitable toughening mechanism for any possible stress history, but strong enough that the elastic properties of the cross-linked network are also optimized.

Hybrid hydrogels with both covalent and noncovalent cross-links provide a tough hydrogel design that can resist creep and improve fatigue resistance.[21−24] One limitation of most hybrid hydrogels is that the permanent bulk shape of the hydrogel is fixed during the formation of the covalent cross-links, which prevents the hydrogel shape to be modified post polymerization.[25] To enable reprocessing of the hydrogel into new complex shapes while maintaining the potential for elasticity recovery, a second, stronger reversible cross-link can be introduced to a supramolecular hydrogel.[19] This has the advantage over single supramolecular network hydrogels, in that the weaker physical network optimizes the energy dissipation, while the stronger physical network improves the elastic nature of the hydrogel. Dual physical cross-link hydrogel systems have been designed to exhibit excellent toughness and fatigue resistance,[26−29] as well as self-healing characteristics.[14,16,30,31]

Gong and co-workers reported a hydrogel with hydrophobic and hydrogen bonds that exhibits high fracture stress (10.5 MPa) and fracture energy (2.85 MJ/m^2).[26] The difference in the lifetimes of the different supramolecular bonds produced 85% recovery of the energy dissipation capacity after a loading−unloading cycle.[26] However, the high stiffness of that hydrogel limited the self-healing efficiency.[26] Alternatively, Jia et al.[29] prepared a poly(ethylene glycol)-modified polyurethane hydrogel with dipole−dipole and hydrogen-bonding networks that exhibited rapid healing and reasonably good fracture resistance (2.49 MJ/m^2). Schäfer et al.[32] reported self-healing hydrogels based on hydrogen bonds and reversible Diels−Alder covalent bonds. Those prior results demonstrate the potential utility of multiple supramolecular network hydrogels, but neither do they discuss the microstructure of such hydrogels nor do they consider the synergy of the two networks. Network topology and connectivity have previously been shown to be important for determining the properties of DN hydrogels;[6] so, it would not be surprising if the relaxation behavior of the different physical bonds in multiple supramolecular network cross-links affected each other and influenced properties such as toughness. Shull and co-workers demonstrated the ability of divalent salts to increase the elastic modulus of a triblock copolymer hydrogel by orders of magnitude.[33] In this case, the end blocks of the copolymer formed hydrophobic cross-links, while the ionized mid-block enabled ionic cross-links. Interestingly, the hydrogel cross-linked by sufficient Ca^{2+} provided excellent fatigue resistance over multiple loading cycles, but the Zn^{2+} cross-linked hydrogel only partially recovered.[33] Although this prior study demonstrated the potential of dual cross-linked hydrogels to provide a combination of toughness and fatigue resistance, these have required relatively high concentrations of divalent ions, but immersion in physiologically relevant aqueous solutions will likely lead to changes in the ion composition and degradation in the desired mechanical properties. Thus, it would be beneficial if this combination of properties could be achieved at relatively low concentrations of divalent ions.

Although there is now a reasonably large literature on tough and self-healing supramolecular hydrogels, in general, the microstructure characterization of those systems is lacking. Our research on hydrophobically modified hydrogels based on statistical copolymers of a water-soluble monomer and a fluoroacrylate monomer indicates that those hydrogels form a core−shell microstructure with fluoroacrylate nanodomains surrounded by a thin shell of a water-depleted layer of the water-soluble segment dispersed in a continuous phase of the water-swollen water-soluble polymer.[18,34−37] The hydrophobic nanodomains serve as physical cross-links, and the reversible nature of the hydrophobic bonds within the nanodomains provides a robust mechanism for toughening the hydrogel. Unfortunately, the well-characterized nanostructure of those hydrogels is an exception within the hydrogel literature. It is very likely that many of the other supramolecular hydrophobically cross-linked hydrogels that have been reported have similar microstructures and that it is important with regard to the mechanisms of toughening and self-healing, since a nanostructured cross-link based on hydrophobic associations may contain as many as 100 physical bonds.[35,38] As such, the toughening, self-healing kinetics, and creep behavior of a supramolecular hydrogel with a nanostructured cross-link are likely to be much different from those of a supramolecular hydrogel with discrete physical bonds (such as divalent cation cross-links[12]). For example, breaking a single cross-link in a nanostructured hydrogel provides an energy release mechanism but keeps the microstructure of the hydrogel essentially intact, since the complete breaking of the network would require the cooperative breaking of many physical bonds to completely eliminate the nanodomain.[39] The dynamics associated with the rearrangement of the segments in the nanodomain under deformation determined from small-angle X-ray scattering (SAXS) can provide some mechanistic insights into rate-dependent mechanical properties, as the changes in the nanostructure during deformation are tempered by the relaxation processes.[40] In contrast, the dynamics for a supramolecular hydrogel where the cross-links are based on 1:1 interactions would be much simpler, in that the physical bond is either intact or broken and if broken, the network chains are then free to move and exhibit plastic flow.

This paper considers the changes of the microstructure, self-healing behavior, and mechanical properties of a statistical copolymer of hydroxyethyl acrylate (HEA), 2-(*N*-ethylperfluorooctane-sulfonamido)ethyl methacrylate (FOSM), and zinc diacrylate (ZnA). Scheme 1 illustrates the structure of the monomers used. The hydrogel formed from this terpolymer consists of two supramolecular networks based on ionic and hydrophobic bonds. Although ionic bonds are usually stronger than hydrophobic bonds, typically, the multivalent ions responsible for the cross-links are present at

Scheme 1. Chemical Structure of the Three Monomers Used: HEA (Hydrophilic Matrix), FOSM (Hydrophobic Cross-Links), and ZnA (Ionic Cross-Links)

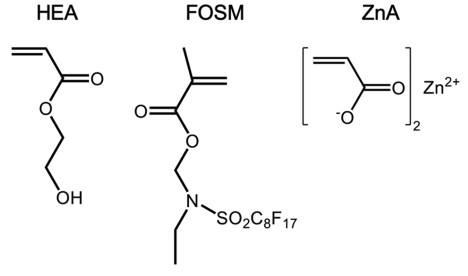

DOI: 10.1021/acs.macromol.9b00830
Macromolecules 2019, 52, 6055−6067

Table 1. Structural Properties of the HF*x* [from Small-Angle Neutron Scattering (SANS)] and HFZ (from SAXS) Hydrogels at 22 °C[a]

hydrogel	$[FOSM]_{cp}$ (mol %)	$[FOSM]_{hg}$ (mmol %)	d_{c+s} (nm)	t_s (nm)	d_c (nm)	d_{c-c} (nm)	G_N (kPa)	S	ν_e (mol/m^3)
HF10	9.91	6.96	3.45	0.48	2.49	6.49	70.1	2.42	79.7
HF21	21.2	33.7	2.41	0.43	1.55	5.53	287	1.42	269
HF30	30.2	207	4.23			3.26	405	1.03	331
HFZ	9.87	8.64				6.79	254	2.12	278

[a] $[FOSM]_{cp}$ = FOSM content in the copolymer/terpolymer; $[FOSM]_{hg}$ = FOSM content in the hydrogel; d_{c+s} = average diameter of the core−shell nanodomains; t_s = average thickness of the nanodomain shell; d_c = average nanodomain core diameter: $d_c = d_{c+s} - 2t_s$; d_{c-c} = average center-to-center distance between neighboring FOSM nanodomains; G_N = the storage modulus at a frequency of 100 rad/s and a strain amplitude of 0.25%; S = swelling ratio of the hydrogel.

large excess to promote their binding with the polymer.[33,41] The complexation of Zn^{2+} to polyacrylic acid (PAA) can be quantified through its equilibrium binding constant[42] or its apparent dissociation constant.[43] These have demonstrated that the Zn^{2+} binding to PAA is stronger than for Ca^{2+},[42,44] with chemical binding, not electrostatics dominating at low degrees of polymer dissociation.[43] However, here, we demonstrated that when the Zn^{2+} concentration is stoichiometric for the acrylate as is the case for ZnA, the copolymer of HEA and ZnA is soluble in water despite the expected network structure that should arise from the multifunctional ZnA (Scheme 1). We attribute this solubility to the reversibility of the divalent ionic bond[45] and the stoichiometric concentration of Zn^{2+} present that leads to a small number of free acrylates due to the equilibrium nature of the binding.[42,43] Despite the inability of these ionic cross-links to inhibit the solubility of the polymer alone, the inclusion of ZnA in a hydrogel based on hydrophobic interactions (terpolymer) significantly increased the elastic modulus of the hydrogel, though it also increased the water absorption compared with a purely hydrophobically modified hydrogel with the same modulus. These terpolymer hydrogels also exhibit improved creep resistance compared with single hydrophobic network copolymer hydrogels. These results provided new insights into the cooperative relaxation behavior of dual physically cross-linked hydrogels.

EXPERIMENTAL SECTION

Materials. 1,4-Dioxane (≥99.0%) was obtained from Sigma-Aldrich. Deuterated chloroform ($CDCl_3$, 99.8% D) and deuterated acetone (acetone-d_6, 99.9% D) were purchased from Cambridge Isotope Laboratories, Inc. Zinc diacrylate (ZnA) was obtained from Scientific Polymer Products, Inc. These chemicals were used as received. 2-(*N*-Ethylperfluorooctane-sulfonamido)ethyl methacrylate (FOSM, ≥85.0%) was purchased from BOC Sciences and recrystallized from methanol. Hydroxyethyl acrylate (HEA, ≥96.0%) was obtained from Scientific Polymer Products, Inc., and the hydroquinone inhibitor in the HEA was removed with a DHR-4 column (Scientific Polymer Products, Inc.). 2,2′-Azobis(2-methylpropionitrile) (AIBN, ≥98.0%), obtained from Sigma-Aldrich, was recrystallized from methanol.

Polymer Synthesis. Statistical copolymers of HEA−FOSM and HEA−ZnA were synthesized by free-radical solution polymerization at 60 °C. The chemical structure of these monomers is shown in Scheme 1. Solutions of HEA and FOSM or HEA and ZnA in 1,4-dioxane were sparged with dry nitrogen for 1 h. The free-radical initiator, AIBN, was dissolved in 10.0 g 1,4-dioxane, and the solution was sparged with dry nitrogen for 2 min before adding it to the monomer solution at 60 °C to initiate polymerization. The reaction was terminated after 36 h by cooling down to room temperature and exposing the solution to air. The reaction solution was concentrated to ≈40% of its original volume with a rotary evaporator at 40 °C and a reduced pressure of 16 kPa and then precipitated in 600 mL diethyl ether at 0 °C. The copolymer product was dried under vacuum at 50 °C for 48 h. The feed composition and yield of these copolymers are summarized in Table S1. The nomenclature to describe the hydrogels associated with the HEA−FOSM copolymers and HEA−ZnA copolymers are HF*x* and HZ*x*, respectively, where *x* denotes the FOSM or ZnA concentration (mol %) of the dry copolymer rounded to the nearest integer.

The HEA−FOSM−ZnA terpolymer, denoted HFZ, was synthesized by an analogous free-radical solution polymerization with 10.5 g HEA, 7.2 g FOSM, and 2.3 g ZnA dissolved in 170 mL 1,4-dioxane in a round-bottom flask. AIBN (0.0148 g) dissolved in 10.0 g dioxane was used to initiate the polymerization. The reaction conditions for the terpolymer were identical to those used for the copolymers.

Proton Nuclear Magnetic Resonance (^{1}H NMR) Spectroscopy. The composition of the copolymer and terpolymer was determined by solution ^{1}H NMR spectroscopy with a Varian Mercury-300 NMR, Figures S1−S3. For NMR, the HEA−FOSM copolymer was dissolved in $CDCl_3$, the HEA−ZnA was dissolved in dimethyl sulfoxide-d_6, and the terpolymer was dissolved in acetone-d_6. The composition of these polymers is listed in Table 1. The target FOSM concentrations were 10, 20, and 30 mol % for the HF10, HF21, and HF30, which are similar to the experimentally determined compositions (Table 1). The target for the HFZ terpolymer was 10 mol % FOSM and 20 mol % of ZnA. The target composition of the HFZ was selected to allow for direct examination of the effect of the zinc acrylate (substitution of ZnA for HEA in HF10 and of FOSM for HEA in HF30). The HF21 was included as it has mechanical properties (shear moduli) most similar to those of the HFZ hydrogel.

Hydrogel Preparation. The HF*x* hydrogels were prepared by vacuum (≈100 kPa) compression molding the dry copolymer into ≈0.50 mm thick sheets at 150 °C with a compressive stress of 5.6 MPa for 2 h using a Technical Machine Products 35 t vacuum molding machine. The copolymer films were then swollen with an excess of type 1 ultrapure water (Milli-Q, Millipore) for at least 14 days at room temperature. The mass of the hydrogel was monitored every 24 h using a Mettler Toledo XS104 Excellence XS analytical balance to ensure that the hydrogel reached equilibrium. Equilibrium swelling was assumed to be achieved when the mass change over a 48 h period was <3%. The dry copolymer mass and the equilibrium swollen mass were used to calculate the swelling ratio, *S*, which is the mass of the hydrated copolymer normalized by the original dry mass. The HZ30 copolymer dissolved in water; so, it was not possible to obtain a hydrogel with that material.

The high concentration of strong ionic cross-links in the dry HFZ terpolymer produced a very high viscosity that made melt molding difficult. However, swelling the HFZ terpolymer with Milli-Q water for 24 h (≈50 wt % water) sufficiently weakened the ionic bonds and sufficiently decreased the viscosity so that the water-swollen HFZ could be compression-molded into ≈0.50 mm thick sheets with a 35 t molding machine (Technical Machine Products) at 60 °C using a compressive stress of 16 MPa for 30 min. After pressing, the HFZ film was swollen at room temperature to equilibrium in an excess of type I ultrapure water, following the same procedure as previously described for the copolymer hydrogels.

Small-Angle Scattering. Small-angle neutron scattering (SANS) was performed on the HF*x* hydrogels enclosed in titanium liquid cells,[46] using the NGB 30 m SANS beamline at the NIST Center for

DOI: 10.1021/acs.macromol.9b00830
Macromolecules 2019, 52, 6055−6067

Neutron Research in Gaithersburg, MD. The neutron wavelength was λ = 0.6 nm with a wavelength spread $\Delta\lambda/\lambda$ of 14%, and the beam diameter was 1.91 cm. Excess solvent (H_2O/D_2O) was added to cover the hydrogel sample to ensure that the sample remained fully hydrated during the SANS measurements. Three sample-to-detector distances, 1.33 m (with seven neutron guides), 4.00 m (with five neutron guides), and 13.2 m (with one neutron guide), were used to provide a wide scattering vector (q) range of 0.300−4.71, 0.0854−0.830, and 0.0343−0.232 nm^{-1}, respectively. Hydrogels were prepared by swelling the copolymers with either D_2O or a (23.5/76.5 v/v) mixture of D_2O/H_2O. The reason for the different isotopic water composition was the expectation for a core−shell nanostructure of FOSM nanodomains surrounded by a water-depleted HEA shell, which has been observed for similar hydrogels.[34,37,47] The different compositions were selected for contrast-matching of various parts of the nanostructure[35,36] for the SANS measurements. Diameter circular disks (≈2.0 cm) were cut from hydrogel films for the measurements. Igor Pro 6.37 was used for the data reduction and analyses, following the procedures described by Kline.[48]

The structure of the HFZ hydrogel was elucidated from small-angle X-ray scattering (SAXS) measurements on beamline 11-BM CMS using 13.5 keV X-rays (λ = 0.0918 nm) at the National Synchrotron Light Source II (NSLS II) at Brookhaven National Laboratory in Upton, NY, with a sample-to-detector distance of 2.02 m and a Dectris Pilatus 2 M detector (pixel size = 172 μm × 172 μm). The HFZ hydrogel film was cut into a 27 mm × 5.5 mm slab and wrapped with an ∼0.02 mm thick Kapton polyimide film (American Durafilm) to minimize water loss during the X-ray experiments. The X-ray exposure time was 5 s. The background scattering (from Kapton films around the hydrogel and in the beamline) was subtracted from the raw scattering data, and the beam stop and the gaps between detector elements were masked to obtain corrected two-dimensional SAXS data. These data were circularly averaged to obtain one-dimensional scattering patterns as a function of q ($q = 4\pi\sin(\theta)/\lambda$, where λ = wavelength and θ is one-half of the scattering angle), using the Nika package for Igor Pro 6.37.[49]

As was mentioned above, the nanostructure of the HFx hydrogels consisted of shell−core nanodomains with an FOSM core diameter of 1.74−2.63 nm surrounded by a water-depleted 0.45−0.47 nm thick HEA shell dispersed in a water-swollen poly(HEA) continuous phase based on fits of the SANS data to a broad peak model.[47] The average separation of the nanodomains was 6.49−5.53 nm as the FOSM concentration increased from 10 to 21 mol %. That hydrogel microstructure was also similar to previously studied *N*,*N*-dimethylacrylamide (DMA)/FOSM hydrogels.[35,36] The nanodomains serve as multifunctional cross-links in those hydrogels. The D_2O/H_2O mixture contrast-matched the water-swollen HEA phase, and scattering from this mixture provided only information about the FOSM core of the nanodomains. For the hydrogels swollen in D_2O, the SANS and SAXS data were initially fit to the broad peak and correlation length models, which were used previously to describe the structure of similar hydrogels.[36,37,40,47] In some cases, the number of terms in the models required for the fit of the scattering data was dependent on the copolymer composition used in the hydrogel. These results are shown in the Supporting Information to provide direct comparisons to prior SANS and SAXS characterizations of similar random copolymer-based hydrogels (Figure S4). To avoid overfitting of the data due to the overlap in the structural levels determined from the series of broad peak and correlation length models, the unified model developed by Beaucage was used to fit all of the scattering curves.[50] For these hydrogels, the shell−core nanodomains can be considered as weakly correlated particles so that the scattered intensity is given as[51]

$$I(q) = \sum_{i=1}^{n} \frac{\left(G_i \exp\left(\frac{-q^2 R_{g,i}^2}{3}\right) + B_i (q_i^*)^{-P_i}\right)}{1 + p_i \theta_i(q)} + bkg \qquad (1)$$

where $\theta_i(q) = 3\frac{\sin q\zeta_i - q\zeta_i \cos q\zeta_i}{(q\zeta_i)^3}$, $q^* = \frac{q}{\left\{\mathrm{erf}\left(\frac{k_i q R_{g,i}}{\sqrt{6}}\right)\right\}^3}$, n reflects the number of structure levels, G_i reflects the contrast and includes the number concentration of structural units, $R_{g,i}$ is the radius of gyration of the structural unit, B_i includes the contrast and characteristic sizes to the structure, P is related to either the surface of the structure (P > 3) or mass fractal scaling of the structure (P < 3), p_i is the packing factor with a maximum value of 5.92 for closed packed, ζ_i is the correlation length between particles, and k_i equals approximately 1.06 for P = 2 and 1.0 for P > 3.

For these hydrogels, the primary structural unit is the FOSM aggregates; so, $R_g^2 = 0.6R^2$ and $B = \frac{9G}{2R^4}$. The scattering contrast is related to either the neutron scattering length densities (b) of the components for SANS or the electron density (ρ_e) for SAXS. For the HF hydrogels, the applicable b's are 1.189×10^{-6} Å^{-2} (HEA), 2.830×10^{-6} Å^{-2} (FOSM), -0.561×10^{-6} Å^{-2} (H_2O), and 6.393×10^{-6} Å^{-2} (D_2O). For the HFZ hydrogel, the applicable ρ_e's are 10.063×10^{-6} Å^{-2} (HEA), 12.656×10^{-6} Å^{-2} (FOSM), 7.380×10^{-6} Å^{-2} (Zn^{2+}), 8.876×10^{-6} Å^{-2} (ZnA), and 9.469×10^{-6} Å^{-2} (H_2O). The fits of the scattering profiles were performed in Irena using Igor Pro 6.37.[52]

Rheological Measurements. The linear viscoelastic (LVE) shear properties, the stress relaxation following a step strain of 6%, creep, and creep recovery of the hydrogel samples were measured with a TA Instruments ARES-G2 rheometer using 8 mm parallel plates and a water reservoir containing 10.0 mL of deionized water to prevent hydrogel dehydration. To prevent slipping during the rheological measurements, serrated plates were used for all measurements, and a compressive force of ≈0.6 N was applied to the hydrogel samples. The LVE response region of the hydrogel samples was determined by a strain sweep with a frequency (ω) of 1 rad/s and strains (γ) between 0.01 and 1%. A strain amplitude of 0.25%, which was within the LVE region for all hydrogels, was used for dynamic shear measurements with ω ranging from 0.1 to 100 rad/s. The creep and recovery properties of the HFx and HFZ hydrogels were measured by the application of a constant stress of 300 Pa (within the LVE region) for 300 s to measure creep, followed by the removal of the stress and monitoring the strain recovery for an additional 300 s.

The effective cross-link densities of the hydrogels, υ_e, at room temperature were estimated from the theory of rubber elasticity, eq 2[53]

$$\upsilon_e = \frac{G_N}{\left(1 - \frac{2}{f}\right)\bar{R}T\left[1 + \frac{\{S-1\}\rho}{d}\right]^{-2/3}} \qquad (2)$$

where G_N is the plateau modulus estimated from the storage modulus, G', measured at ω = 100 rad/s and γ = 0.25%, $\bar{R}$ is the gas constant, T is the absolute temperature, S is the swelling ratio, ρ is the density of the copolymer, d is the density of the solvent, and f is the average functionality of the cross-links, which is 4 for the FOSM−FOSM and COO^-Zn^{2+}−OOC cross-links since each cross-link by two associating polymer chains produces four network chains. Note that eq 2 makes no assumptions as to the chemistry or nature (covalent or physical) of the cross-links and is applicable to permanent or temporal cross-links such as supramolecular or chain entanglements as long as those cross-links are in effect at the conditions at which G were measured. In this case at the low strain amplitude and high frequency used to measure G', the physical cross-links were expected to be intact. The functionality of the cross-links was assumed to be 4 based on the basic fundamental interaction between two ionic acrylate groups bridged by Zn^{2+} and the hydrophobic association of two FOSM groups. It should be noted that eq 2 assumes a homogeneous network. The scattering profiles (Figure S4) show an upturn at low q associated with large-scale heterogeneities that are typically associated with fractal objects arising from the differences in the cross-link density. However, the influence of these large-scale inhomogeneities, relative to the size between the cross-links (as suggested by the small spacings between the cross-links, Table 1), on the estimation of the cross-link

DOI: 10.1021/acs.macromol.9b00830
Macromolecules 2019, 52, 6055−6067

density should be small. The effect of these large-scale heterogeneities likely will be significant during nonlinear deformation, which was not examined in this work. The estimated cross-link densities of the HF*x* and HFZ hydrogels are summarized in Table 1. One can also use the size for the FOSM domains obtained from scattering to estimate an overall functionality for the hydrophobic cross-links that contain many (100's) FOSM units.[35,36] However, this requires additional assumptions about the relative effectiveness of each FOSM unit as a cross-link. Although there is a quantitative difference in the estimated cross-link density based on assumptions of the FOSM cross-link functionality, the choice of assumptions that determine the functionality does not impact conclusions about the cross-link density differences between the copolymer hydrogels examined.

The stress relaxation behavior of HF*x* and HFZ hydrogels was monitored for 10^4 s after the application of a step shear strain of 6.0%. The data were fit to a generalized Maxwell model (GMM), eq 3

$$\frac{\tau(t)}{\tau_o} = \sum_{i=1}^{N} c_i \, e^{-t/\lambda_i} \tag{3}$$

An alternative form for the generalized Maxwell model that included a term for residual stress in the hydrogel was also examined (Figure 4)

$$\frac{\tau(t)}{\tau_o} = \sum_{i=1}^{N} c_i \, e^{-t/\lambda_i} + R \tag{4}$$

where $\tau(t)$ is the stress at time t, τ_0 is the instantaneous stress following the step strain, c_i is the fractional contribution of the ith Maxwell element, λ_i is the relaxation time associated with the ith Maxwell element, and R is the residual normalized stress. In the latter case, the residual stress term arises from relaxation times much greater than the experimental time (10^4 s) so that those relaxation modes behave like covalent bonds, preventing any relaxation of the stress associated with those modes. The number of Maxwell elements (N) used to fit the stress relaxation data was varied between 4 and 7, depending on the minimum number of elements that were needed to obtain the good fits of eqs 3 and 4 to the data.

The self-healing properties of the nanostructure of the hydrogels were assessed by the recovery in the storage modulus (G') after the application of a large strain. Oscillatory shear with a strain amplitude of 0.25% and ω = 1 rad/s was used to measure G' prior to the application of a strain sweep with ω = 1 rad/s and γ = 1−100%. Following the strain sweep, the time-dependent recovery of G' was measured by oscillatory shear with γ = 0.25% and ω = 1 rad/s.

RESULTS AND DISCUSSION

Figure 1a shows images of the different hydrogel samples in their fully hydrated state. After melt-pressing of the copolymer, all specimens were initially translucent similar to the HF30 shown in Figure 1a. Upon swelling, the transparency of the samples decreased with the highly swollen HF10 becoming opaque. The decrease in transparency was attributed to density heterogeneities from the formation of water-rich and water-lean regions within the hydrogels (i.e., an inhomogeneous distribution of water),[36] which produces light scattering due to the differences in refractive index between water- and polymer-rich regions. Similar observations have been reported for other physically[35,36,54] and covalently[38,55] cross-linked hydrogels. HF21 was less opaque than HF10 and HFZ, which suggests that it had a more homogeneous microstructure. The transparency of the HF30 is a consequence of its limited water uptake (3 wt %). That sample, which was not technically a hydrogel, was brittle compared to the flexible nature of the other HF*x* and HFZ hydrogels.

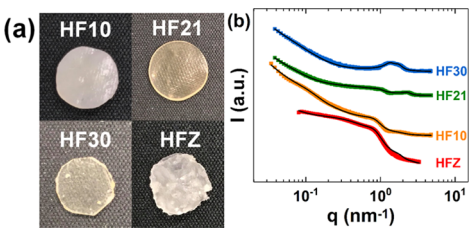

Figure 1. (a) Optical images of HF*x* and HFZ hydrogel samples in their fully (equilibrium) hydrated state. (b) Small-angle scattering patterns of the HF*x* and HFZ hydrogels at 22 °C. SANS is used to characterize the D_2O-swollen HF*x* hydrogels, while SAXS is used to characterize the HFZ. The solid curves are the fits to eq 1.

Structure of Hydrogels from Scattering and Small-Amplitude Oscillatory Shear. Figure 1b shows the SANS patterns associated with the structure of the HF*x* hydrogels and SAXS profile for the HFZ hydrogel. The increased scattering at low q is associated with differences in the water content at larger length scales that is consistent with the cloudiness of the materials. The peaks in the scattering patterns at $q_0 \approx 0.968$, 1.14, 1.93, and 0.925 nm^{-1} for HF10, HF21, HF30, and HFZ, respectively, correspond to the average center-to-center distance between neighboring FOSM nanodomains ($d_{c\text{-}c}$),[34,37,54] $d_{c\text{-}c} = 2\pi/q_0$. Those values and the details of the nanostructures obtained from fits of the scattering data for each of the hydrogels (Figures 1b and S4) are listed in Table 1. Increasing the FOSM content in HF*x* hydrogels decreased $d_{c\text{-}c}$, partly because of the increase in the volume fraction of FOSM nanodomains and partly because of the reduction in the water swelling of the continuous HEA phase of the hydrogel. Notably, for the HFZ hydrogel, which had a similar FOSM content as the HF10 hydrogel, ≈10 mol %, $d_{c\text{-}c}$ of HFZ was larger than that of HF10 (Table 1) despite a lower water swelling ratio for the HFZ. This suggests that the incorporation of ionic cross-links increases the average spacing between FOSM nanodomains. Previously, the inclusion of ionic species at the junction of a neutral diblock copolymer was shown to increase the domain spacing in the bulk copolymer as well.[56]

The nature of the cross-link in the hydrogel influences its microstructure, as shown from the small angle scattering patterns. To better understand the differences, the structures of the hydrated copolymers and terpolymers examined here, as well as more conventional covalently cross-linked hydrogels, are shown schematically in Figure 2. Covalently cross-linked hydrogels are formed by the inclusion of multifunctional monomers that provide the cross-link points (circled in red in Figure 2a). In contrast to these single monomer cross-link, the association of the hydrophobic FOSM in the HF*x* hydrogels is composed of many monomers (as illustrated by the purple circle in Figure 2b), which provides sufficient contrast to resolve the cross-link structure with SANS and SAXS, as demonstrated in Figure 1. The copolymer of HEA and ZnA dissolved in water; so, the ionic bridge with ZnA does not form a long-lived network, as shown in Figure 2c. For the terpolymer, both ionic and hydrophobic associations are present on each polymer chain. This leads to the ZnA being confined between the FOSM domains (Figure 2d) and this increases the d-spacing between the FOSM slightly (Table 1), as determined from the scattering. We have drawn the terpolymer copolymer with the ionic ZnA being associated in the hydrogel (Figure 2d), as will be discussed later.

The linear viscoelastic (LVE) properties of these hydrogels provide additional insight into the structure of the HF*x* and HFZ hydrogels. As the scattering primarily provided

DOI: 10.1021/acs.macromol.9b00830
Macromolecules 2019, 52, 6055−6067

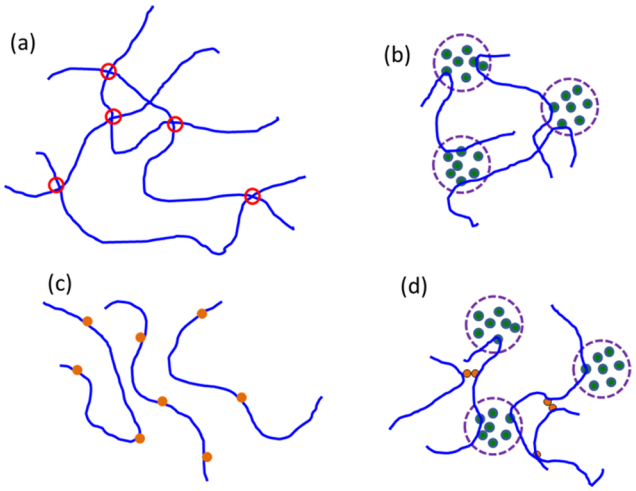

Figure 2. Schematic illustrating the microstructure associated with (a) conventional covalently cross-linked hydrogels (with the cross-links circled in red), (b) HF*x* hydrogels cross-linked by FOSM aggregates where the FOSM groups are shown in green, and the effective size of the cross-link is shown by the purple dashed circle, (c) HZ30 with Zn acrylate associable units (shown by the orange dots) that is water-soluble, and (d) the HFZ hydrogel that includes two physical cross-links. Note that the schematics are not drawn to scale. Only some of the chains involved in forming the FOSM aggregates are shown for clarity.

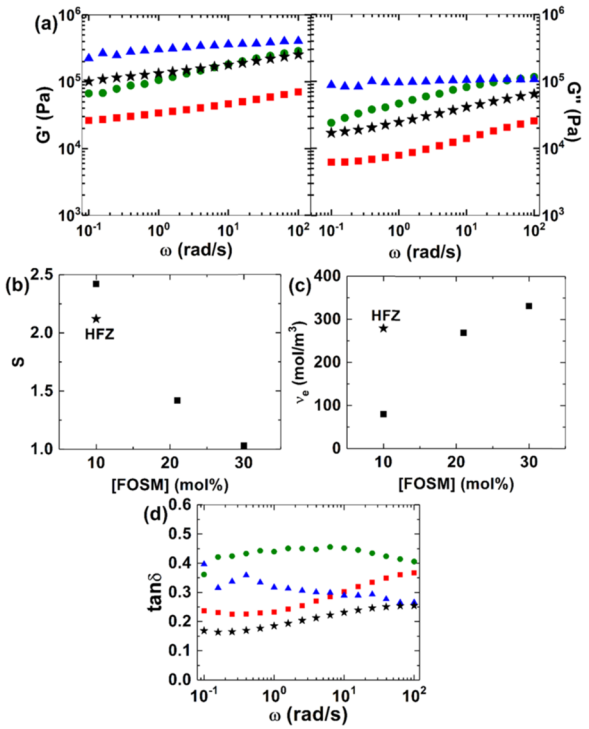

Figure 3. (a) Angular frequency (ω) dependence of the storage modulus (G') and loss modulus (G'') of (red box solid) HF10, (green circle solid) HF21, (blue triangle up solid) HF30, and (star solid) HFZ hydrogels. From gravimetric measurements, the (b) swelling ratio (S) of (box solid) HF*x* and (star solid) HFZ hydrogels was determined. (c) Estimated cross-link density (ν_e) of (box solid) HF*x* and (star solid) HFZ hydrogels was calculated from G' at 100 Hz. (d) Angular frequency (ω) dependence of the loss factor ($\tan\delta$) for (red box solid) HF10, (green circle solid) HF21, (blue triangle up solid) HF30, and (star solid) HFZ hydrogels.

information about the distance between the FOSM aggregates, the LVE properties complement this structural understanding through the mechanical response that provides insight into the network formed in these hydrogels. Figure 3a illustrates that all of the hydrogels exhibit a solid-like behavior with the storage modulus (G') always greater than the loss modulus (G'') within the frequency range examined (0.1−100 rad/s). The gels were viscoelastic with frequency-dependent G' and G''. For a fixed frequency, G' increased with increasing FOSM content for the HF*x* hydrogels, which is consistent with increasing cross-link density at higher FOSM concentrations (see eq 2). By comparing HF10 and HFZ hydrogels that contain the same FOSM content in the polymer, the storage modulus was increased with the addition of ZnA. That result is qualitatively consistent with the previously reported addition of Zn^{2+} to a hydrophobically cross-linked hydrogel that more dramatically increased the modulus of a triblock copolymer-based hydrogel.[33] However, in the prior case, an excess of Zn^{2+} was added relative to methacrylic acid on the copolymer, where the concentration of Zn^{2+} was used to control the mechanical properties of the hydrogel.[33] In this work, the total Zn^{2+} present is stoichiometric to the acrylic acid based on the structure of the zinc diacrylate monomer (Scheme 1).

The water content of the hydrogels (S = mass of the hydrogel/mass of the dry polymer), as well as cross-link density estimated from eq 2, is shown as a function of the FOSM content in Figure 3b,c, respectively. For the HF*x* hydrogels, the swelling ratio decreased monotonically and the effective cross-link density as determined from rheology increased with increasing FOSM content. The HFZ hydrogel contained the same concentration of FOSM as did HF10, but also 22.5 mol % ZnA to provide ionic supramolecular cross-links in addition to the hydrophobic cross-links from the FOSM groups (Figure 2d). By comparing the HFZ to the HF10 hydrogel where the FOSM content is identical, the plateau modulus of the HFZ hydrogel increased by about 260% (Figure 3a) and the swelling ratio decreased by about 12%. According to eq 2, both of these results should be associated with increased cross-link density of the hydrogel. At low concentrations of divalent cations, Shull and co-workers reported that the effect of the ions was only to deswell their triblock copolymer-based hydrogel but no increase in elastic modulus is observed that would be demonstrative of intermolecular crosslinking by the Zn^{2+}.[33] This observation appears to be counter to the HFZ hydrogel examined here, where the hydrogel deswelled slightly, but G' increased significantly. As shown in Figure 3c, the cross-link density and plateau modulus of the HFZ hydrogel were comparable to those of the HF21 hydrogel, which only possessed hydrophobic cross-links, but the swelling ratio of the HFZ was about 50% greater than that of HF21.

To explain the differences in the behavior for the HFZ and the triblock hydrogels of Shull at low Zn^{2+} concentrations,[33] the structures of these materials can be examined. First, the triblock contained methacrylic acid and methyl methacrylate as the hydrophilic and hydrophobic monomers only, respectively, with the association of the methacrylic acid with Zn^{2+} controlled by the solution concentration of Zn^{2+}. The HFZ contains a monomer (ZnA) for the ionic functionalization that is not present in the HF*x* hydrogels; so, the associative differences with the acrylic acid groups versus HEA will have some impact on the mechanical response in the HFZ hydrogel.

DOI: 10.1021/acs.macromol.9b00830
Macromolecules 2019, 52, 6055−6067

Second, the size of the hydrophilic domains between the hydrophobic cross-links is expected to be significantly smaller for the HF*x* and HFZ hydrogels. This will likely confine the ionic species present in the HFZ near hydrophobic surfaces (FOSM nanodomains), which can influence the properties of water[57] and ions.[58] Third, the architecture of the polymers is significantly different from the block structure, leading to all of the hydrophobic cross-links originating from the chain ends, whereas the statistical nature of the copolymers (HF*x*) and terpolymer (HFZ) leads to the potential of a single chain being involved with many different hydrophobic cross-links. Recent work has demonstrated an improvement in the toughness of hydrogels based on random copolymers than on triblock copolymers at the same composition,[59] which suggests that the chain architecture may be responsible for the apparent discrepancies in the effect of Zn^{2+} at a low concentration between this work and the earlier work from Shull and co-workers.[33]

Note that for HFZ, the concentration of functional sites (hydrophobic and ionic) was about 34 mol % compared with the 21 mol % hydrophobic groups in HF21, which suggests that not all of the "cross-linkable" ionic sites provided as effective cross-links as the FOSM aggregates in the HFZ hydrogel. That can be explained by the reversibility of these ionic bonds[45] and the equilibrium associated with the binding of Zn^{2+} to acrylic acid.[42,43] Despite this reversibility of the ionic bond, adding the ionic cross-links to the hydrophobically modified hydrogels decreased $\tan\delta$ over the frequency range considered in this study, as shown in Figure 3d. The lower $\tan\delta$ is indicative of the hydrogel having an increased elastic character (note that for a perfectly elastic material, $\tan\delta = 0$). This result indicated a more ideal network for the HFZ hydrogel than for the HF30 material that contains only 3% water.

Stress Relaxation in Physically Cross-Linked Hydrogels. The improved elastic nature of the hydrogel by the incorporation of ionic cross-links is evident from the relaxation dynamics of the network. Note that for a perfectly elastic solid, there is no relaxation of the stress. Figure 4 shows the stress relaxation behavior of the HF*x* and HFZ hydrogels at room temperature (≈22 °C) after the application of a step shear strain of 6.0%. After 3 h relaxation, less than 10% of the original stress remained for the HF10 and HF21 hydrogels. This relatively rapid stress relaxation behavior is attributed to the fast network chain dynamics of the hydrated HEA network chains and the rearrangements of the FOSM nanodomains under stress. Previous in situ SANS experiments for similar amphiphilic copolymer hydrogels indicated that the nanostructure recovered more rapidly in the direction of the applied load and a much slower relaxation of the nanostructure occurred in the orthogonal direction.[37] The latter slow structural relaxation is likely responsible for the small residual stress in the HF10 and HF21 hydrogels after 3 h. This decay in the stress for the HF10 and HF21 hydrogels suggests that the hydrophobic cross-links are only effective for relatively short time scales under an appreciable load and unable to elastically maintain applied stress as observed for a cross-linked network.[60] The stress decay is similar to that typically observed for a viscoelastic liquid, although these hydrogels behave as viscoelastic solids over time scales associated with oscillatory shear measurements (Figure 3d).

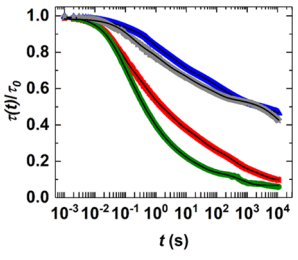

Figure 4. Stress relaxation response for (red box solid) HF10, (green circle solid), HF21, (blue triangle up solid), HF30, and (gray star solid) HFZ hydrogels following a step shear strain of 6.0%. The solid black lines are the fit to the generalized Maxwell model with residual stress (GMMR) with $N = 6$.

Conversely, nearly 50% of the original stress in the HF30 remained after 30 h. That result is presumably a consequence of longer relaxation times due to the higher glass-transition temperature of the poly(HEA) chains with only a small amount of water in the material ($S = 1.03$) and the hydrogen-bonding interactions between the poly(HEA) chains that exist in the relative absence of water. The stress in the HF30 appears to be approaching a plateau at the longest times examined, which would be associated with the viscoelastic solid-like behavior over the time scales examined.

Interestingly, the relaxation behavior of the HFZ hydrogel more closely resembles that of HF30 despite the much higher water content. There is an effective plateau in the stress between 10^2 and 10^3 s, which is indicative of the cross-links in the HFZ being effective over this time scale unlike the hydrophobic aggregates in the HF*x* hydrogels (Figure 4). The change in the shape of the stress relaxation at 25 °C between the HF*x* and the HFZ hydrogels is likely due to different parts of the relaxation spectra being probed. A similar change in the relaxation spectra was observed for the stress relaxation of hydrophobically cross-linked hydrogels when the length of the alkyl side chains was increased from hexyl to dodecyl.[59] For the HFZ hydrogel, the longer effective plateau in the stress (in comparison to the HF*x* hydrogels) points to the efficacy of the ionic bonds produced by the ZnA groups at decreasing the dynamics of the network chains, which itself may be surprising, since poly(ZnA) is water-soluble. The solubility of poly(ZnA) might lead one to believe that the ionic bond between Zn^{2+} and the two carboxylate ions is not effective at such low Zn concentrations.

We primarily attribute the effectiveness of ionic bonds to contribute to the network in the HFZ hydrogels, as demonstrated by the data in Figures 3 and 4, to its nanostructure that provides locally hydrophobic environments separated by <4 nm. Previously, the binding of Cu(II) to acrylic acid-based hydrogels was demonstrated to increase as the hydrophobicity of the hydrogel increased;[61] so, the equilibrium in the Zn^{2+} binding in the HFZ hydrogels was expected to be shifted toward the bound state for effective cross-links. Additionally, a similar enhancement in the efficacy of weak physical cross-links has been reported previously when covalent cross-links are included in hydrogels with heparin and heparin-binding peptides that are physical cross-links.[60] Without covalent cross-links, these polymers with the heparin are water-soluble, but the physical cross-links substantially increase the modulus when included with covalent cross-links.[60] This was attributed to the increased relaxation time for the gel due to the connectivity associated with the covalent cross-links. An extension in the relaxation time for the stress is

DOI: 10.1021/acs.macromol.9b00830
Macromolecules 2019, 52, 6055−6067

Table 2. Fitting Parameters for the GMMR with $N = 6$ for the Stress Relaxation Response of HFx and HFZ Hydrogels

	HF10		HF21		HF30		HFZ	
Maxwell element	c_i	λ (s)	c_i	λ (s)	c_i	λ (s)	c_i	λ (s)
1	0.205	0.0533	0.218	0.0596	0.0411	0.0377	0.123	0.142
2	0.237	0.211	0.201	0.414	0.118	0.619	0.113	1.26
3	0.188	0.867	0.151	2.88	0.121	5.08	0.0873	9.80
4	0.123	4.07	0.125	25.7	0.0834	50.2	0.0878	82.7
5	0.0973	25.7	0.112	302	0.104	349	0.0141	523
6	0.0799	663	0.0830	2.89×10^3	0.0653	4.89×10^3	0.168	1.11×10^4
R	0.0678		0.0967		0.462		0.345	
$\sum c_i$	0.930		0.890		0.533		0.593	
$\sum c_i + R$	0.998		0.987		0.995		0.938	
COD	1.00		1.00		1.00		1.00	

indeed observed here for the HFZ hydrogel, which is consistent with this explanation for a dual cross-linked hydrogel with covalent cross-links.[60]

To quantify the stress relaxation behavior of these hydrogels, a nonlinear least-squares regression was used to fit the generalized Maxwell model (GMM), eq 3, or generalized Maxwell model with residual stress (GMMR), eq 4, to the relaxation data for each hydrogel. Although there are several models that can describe the stress relaxation of polymers, a discrete relaxation time model was selected due to its simplicity and clear physical significance of the parameters obtained from the fit. Mathematically, a series of exponential functions that describe the relaxation processes can be used to fully describe the rheological properties of a material.[62] The quality of the fit was assessed by calculating $\sum_{i=1}^{N} c_i$ or $\sum_{i=1}^{N} c_i + R$, which ideally should be unity, and the goodness of the fit quantified by the coefficient of determination (COD). The number of Maxwell elements used was the fewest that provided a good fit of the data[62] over the entire time of the experiment, as judged by COD $\geq$ 0.999. Figure S5 shows the GMM fits of the stress relaxation data for $N = 4-7$ Maxwell elements, and Tables S3–S6 summarize the values of $\sum_{i=1}^{N} c_i$ and COD for the regression fits. For $N < 6$, the GMM generally failed to adequately represent the short time behavior, due most likely to the failure to include the longest relaxation times for the hydrophobic associations. Fits with $N = 6$ produced COD values of 0.999, Table 2, but even though those fits had high COD, $\sum_{i=1}^{N} c_i < 1.0$, which is a consequence of the model failing to account for very long relaxation times. Adding an additional Maxwell element, i.e., $N = 7$, did not improve the nonlinear regression fits and produced replicate relaxation times for multiple Maxwell elements, indicating that the fit was overparameterized.

Note that the GMM fits showed at least one relaxation time that was longer than the measurement time ($\sim 10^4$ s). The large value of c_i associated with this relaxation that indicated the long relaxation time represented a significant fraction of the stress response, see Tables S3–S6. This result suggests that in addition to the distribution of relaxation times below 10^4 s, there is a second distribution of longer relaxation times that probably arises from the reversible cross-links that is not adequately resolved by these GMM fits. Bonds with relaxation times greater than 10^4 s may be considered permanent cross-links within the time frame of the stress relaxation experiments that were run in this study. As such, the stress relaxation data were fit with a GMMR model with $N = 6$ that included a term for the residual stress, R. This approach better fits the stress relaxation data, and the values of R provide a measure of the effect of the bonds with very long relaxation times on the contribution to the stress in these materials. The fitting parameters and fitted curves associated with the GMMR model are summarized in Table 2 and Figure 4, respectively.

Despite its higher water content, the HFZ hydrogel had longer relaxation times than HF21. Moreover, the fractional contribution (c_i) of the longest relaxation time of HFZ listed in Table 2 was much larger. In fact, the relaxation time distribution (Table 2) for HFZ was comparable to that of the HF30 sample with its very low water content. While for HF10 and HF21, less than 10% stress remained after 10^4 s, 46% of the stress in HF30, and about 35% of the stress in HFZ remained after 10^4 s. Since there were no covalent cross-links in these gels, the viscoelastic behavior should be that of a liquid at sufficiently long times and the stress should eventually relax to zero for the HFx and HFZ hydrogels. This fact indicates that there were much longer relaxation times associated with the dynamics of the gels, especially the HFZ hydrogel, that were not resolved by the stress relaxation analysis discussed above. This conclusion is consistent with the lower value of $\sum_{i=1}^{N} c_i$ for HFZ compared with that for HF10 and HF21 in Table 2. What is particularly remarkable about the stress relaxation behavior of HFZ is the apparent influence of adding the ionic interactions on the dynamics. The ability of these ionic bonds to affect the dynamics of these supramolecular hydrogels provides the opportunity to decouple the mechanical and water swelling behaviors, i.e., high modulus with high swelling ratio, that are not generally possible in a hydrogel with only a single type of physical cross-link.

The ionic bonds are connected to the same network chains as are the hydrophobic bonds. The fast relaxations in a hydrogel network generally can be correlated to the network chain motions and the weaker reversible cross-links. That is, when the network chains are stressed, one would expect the weaker physical bonds to break first. Although the poly(ZnA) dissolves in water, as shown in Table 2, the fastest relaxation in HFZ appears to be slower than that for HFx. The presence of the hydrophobic network affects the dynamics of the ionic cross-links such that their lifetime under stress is much longer than expected. This result is consistent with electron paramagnetic resonance spectroscopic studies that showed increased ion binding with increasing hydrophobicity of the hydrogel environment.[61]

One would normally expect that the slower relaxation processes in the HFx and HFZ hydrogel networks would be

DOI: 10.1021/acs.macromol.9b00830
Macromolecules 2019, 52, 6055–6067

dominated by the dynamics of the hydrophobic nanodomains. The nanodomain cross-links that characterize the hydrophobic network contain ∼100 FOSM groups. As such, the multifunctional cross-links are rather robust, and one expects that the stress in the hydrogel concentrates at the locus of the interface between the poly(HEA) network chain and FOSM group to which it is attached. In principle, the stress in a network chain can be dissipated by releasing individual network chains from a nanodomain cross-link, which requires pulling an FOSM group out of the nanodomain. This process is consistent with the very long relaxation times seen in the stress relaxation behavior, Table 2, and has been previously attributed to an FOSM jumping process, whereby an FOSM−FOSM bond breaks and an individual FOSM group is either pulled out of the nanodomain or it reorganizes with other FOSM groups within the nanodomain.[37,40] However, the slow relaxations of the HFZ hydrogel were even slower than those of the HF*x* hydrogels. This behavior can potentially be attributed to the local charge density from the ionic cross-links that led to an increased penalty for the rearrangement of FOSM nanodomains and/or less chain conformations available for the network due to the ionic cross-links between the FOSM nanodomains.

Microstructure Self-Healing. The rearrangements enabled by noncovalent cross-links should enable self-healing of these hydrogels, but the self-healing process should depend on their viscosity as the molecular-scale flow is necessary to repair the damage. In this case, we consider the self-healing of the microstructure of the hydrogel[18] in contrast to the self-healing of fractures or cuts.[63] For physically cross-linked hydrogels with reversible bonds, the latter is expected when considering viscoelasticity as long as the time for healing exceeds the longest relaxation time for the hydrogel. At these long times, the physically cross-linked hydrogel is effectively a viscoelastic liquid and the material will flow under the applied force (including gravity) like any liquid. Conversely, the healing of the microstructure requires the pathways for the healing to proceed without kinetic traps back to the original structure. Given the propensity of amphiphilic block copolymers to form kinetically trapped nanostructures,[64] it is not evident that the microstructure of these hydrogels will self-heal. To test the healing ability of the HF10, HF21, and HFZ hydrogels, these hydrogels were damaged through a strain sweep at ω = 1 rad/s as the strain amplitude increased from 1 to 100%. The healing was then monitored by low-amplitude oscillatory shear (ω = 1 rad/s) using a strain amplitude of 0.25%. Figure 5 illustrates two cycles of damage and recovery for the different hydrogels. During the first strain sweep, the LVE response of the HF10 hydrogel persisted to approximately 10% strain. From ≈10 to 100% strain, G' of HF10 decreased by 2 orders of magnitude, which is indicative of damage to the network structure in the hydrogel. Based upon prior in situ SAXS measurements during the deformation of similar hydrophobically cross-linked copolymer hydrogels,[40] this damage is likely associated with the removal of individual FOSM units from existing domains to decrease the effective cross-link density with the FOSM domains deformed from spherical to ellipsoidal at a sufficiently high strain rate. As the strain is increased, the strain rate also increases, which impacts the nanostructure of these types of hydrogels.[40] A similar microstructure self-healing has been reported for analogous hydrogels based on dimethylacrylamide and FOSA.[18] Increasing the cross-link density produced a nonlinear behavior (i.e., decreasing G' with increasing strain) at lower strain amplitudes. For HF21 hydrogel, G' decreased by almost 3 orders of magnitude as the strain increased from 1 to 100%. As the HF30 only contained ≈3% water, this material was not examined for its self-healing properties.

In contrast to the HF*x* hydrogels, the HF21 hydrogel maintains its LVE response until ≈10% strain, despite its higher effective cross-link density than HF21 and HF10. Moreover, G' of the HFZ hydrogel only decreased by an order of magnitude when the strain amplitude was increased to 100%. This smaller decrease in G' of HFZ in comparison to HF*x* is attributed to the greater resilience of the physical cross-link network in the system. In addition to the ability of the HFZ to maintain its elastic properties at larger strains, the recovery of the mechanical properties after damage at high strain is important for understanding the self-healing properties of these hydrogels. From Figure 5, the recovery of G' appears relatively rapid (<1 min) for the 100% strain damage for all of the hydrogels examined.

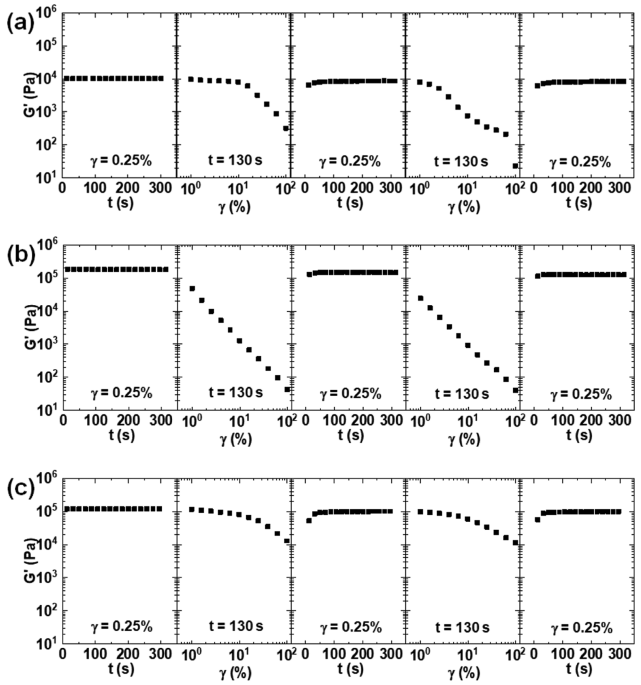

Figure 5. Oscillatory shear with a strain amplitude of 0.25% and a constant ω of 1 rad/s was applied to the (a) HF10, (b) HF21, and (c) HFZ hydrogels before and after the application of large oscillatory strains with amplitudes up to 100%. This process was repeated for two cycles.

Figure 6 more clearly summarizes the recovery of these hydrogels. Immediately following the 100% deformation (time

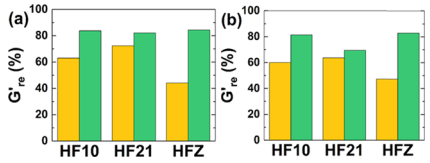

Figure 6. Fraction of the initial storage modulus recovered (G'_{re}) for the HF10, HF21, and HFZ hydrogels (yellow) immediately following large amplitude shear (100% strain) and (green) after 300 s recovery for (a) first and (b) second cycles (strain sweep and 300 s recovery) shown in Figure 5.

DOI: 10.1021/acs.macromol.9b00830
Macromolecules 2019, 52, 6055−6067

resolution of rheometer at 1 rad/s), G' recovers 63% of its initial value for HF10 and 72% for the HF21 hydrogel (Figure 6a). The enhanced recovery in G' for HF21 is consistent with its more rapid stress relaxation (Figure 4). As expected from its longer relaxation times, G' of the HFZ hydrogel only recovered 44% of its initial value immediately after the 100% strain, Figure 6a. G' recovers almost to an identical extent after 100 s (≈84% of the initial value) as the HF10 and HF21 hydrogels, Figure 6a. The slower self-healing of the HFZ hydrogel likely originates from the conformational pinning of the ionic cross-links, which hinders the recovery of FOSM nanodomains. This phenomenon can also explain the longer relaxation times of the HFZ hydrogel than those for HF10 and HF21 hydrogels. This self-healing can be repeated, but there appears to be a gradual decrease in the recovered G' in the second cycle for the HF10 and HF21 hydrogels (Figure 6b). Intriguingly, the recovery of G' did not change much for the HFZ hydrogel on the second cycle.

Creep and Creep Recovery. While the discussions above on stress relaxation revealed the synergistic effect of hydrophobic and ionic cross-links on the mechanical response of the HFZ hydrogel, creep and creep recovery experiments were also performed to further understand the dynamics and rearrangement of the physical cross-links under load[19] and the microstructure self-healing, which depend on the relaxation processes, viscosity, and thermodynamics of the associations. Figure 7a shows the change in strain during the creep of the

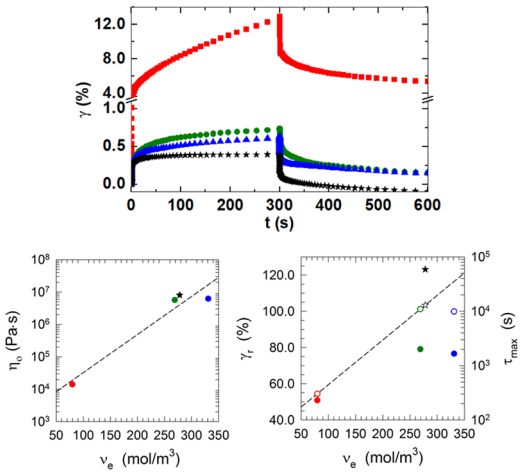

Figure 7. Creep and creep recovery behavior of HF$_x$ and HFZ hydrogels. (a) Creep and creep recovery (stress = 300 Pa) for (red box solid) HF10, (green circle solid) HF21, (blue triangle up solid) HF30, and (star solid) HFZ hydrogels. (b) The zero shear rate viscosity calculated from the creep measurements of (circle solid) HFx and (star solid) HFZ hydrogels. (c) Recoverable strain for (circle solid) HFx and (star solid) HFZ and the maximum retardation time for (circle open) HFx and (star open) HFZ hydrogels.

HFx and HFZ hydrogels with an applied shear stress of τ_o = 300 Pa, which was within the LVE region. After the stress was applied for ≈150 s, all hydrogels achieved a steady-state flow, where the strain rate ($d\gamma/dt$) remained constant. The zero shear rate viscosity (η_0) of the sample is defined as $\eta_o = \tau_o/(d\gamma/dt)$, which is the constant shear stress divided by the slope of the linear portion of the creep curves in Figure 7a, as illustrated by the dashed line for the HF10 hydrogel.

The viscosity of the hydrogels measured from Figure 7a is plotted against the cross-link density, ν_e, in Figure 7b. In the flow regime of the creep experiment, the network is no longer intact; so, in that case, ν_e is considered as the concentration of transient hydrophobic associations, or stickers,[65] rather than cross-links. η_o also depends on the molecular weight of the polymer and the concentration of water in the hydrogel. Although the polymer concentrations in the gel varied from about 0.41 g/mL for HF10 to 0.70 g/mL for HF21, those differences were insufficient to account for the 3 orders of magnitude differences in viscosity shown in Figure 7b. The changes in η_o shown in Figure 7b are primarily attributable to differences in ν_e, and the relationship appears to be linear (dashed line in Figure 7b), though the data were limited. HF10, which had the lowest ν_e, correspondingly had the lowest η_o and exhibited the greatest creep. The zero shear viscosities of HF21 and HF30 were 3 orders of magnitude higher than for HF10. Although η_o for HFZ was about 10% higher than for HF21, the linear relationship indicated by the dashed line in Figure 7a suggests that the higher viscosity of HFZ may be a consequence of the slightly higher ν_e.

The differences in the strain achieved during the creep experiment between the HF10 hydrogel and the HF21 and HFZ hydrogels were mainly due to the difference in their recoverable compliances (2.16×10^{-4}, 1.93×10^{-5} vs 1.27×10^{-5} Pa^{-1} for HF10, HF21, and HFZ, respectively), which is the elastic response manifest in the creep data near t = 0. Also, since HF10 had a lower viscosity, the creep due to viscous flow, at longer times, was much greater than that for the HF21 and HFZ gels. The difference in the strain at the end of the creep experiments for HF21 and HFZ was small, but it appeared to be due to primarily the difference, albeit small, between their viscosities. The recoverable compliances of these two hydrogels were similar, which would be expected since their cross-link densities were within 4%. The viscosity of HFZ was about 10% greater than that of HF21, which may account for the larger strain (~50%) at the end of the creep experiment (t = 300 s) for HF21 than for HFZ. That is, the higher η_0 reduced the total strain of the HFZ hydrogels during creep in comparison to the HF10 and HF21 hydrogels.

Stress recovery data for the three hydrogels after removing the stress at t = 300 s are also shown in Figure 7a. The strain from a creep recovery has two contributions: (1) recoverable strain, γ_r, that is due to the elastic response at the beginning of the creep experiment and (2) nonrecoverable strain, γ_f, that is due to plastic flow or permanent deformation as a result of changes in the microstructure. Figure 7c shows $\gamma_r(t)$ as a function of ν_e. The recoverable strain increased with increasing ν_e, but the data in Figure 7c indicate a large difference between the γ_r values at t = 300 s for HF21 (79%) and HFZ (123%), which had similar values of ν_e. The value of γ_r > 100% may indicate that drift occurred in the transducer during that experiment. Given that issue, the best one can conclude here is that the recoverable strains for HF21 and HFZ were high. The maximum retardation times, $\tau_{max} = \eta_o\gamma_r/\tau_o$, for the hydrogels and HF30 are also plotted in Figure 7c. τ_{max} increased with increasing ν_e. The straight line drawn through the τ_{max} versus ν_e data would seem to indicate that the difference in the maximum retardation time for HF21 and HFZ is due to the small difference in ν_e, a finding that is in contrast to the conclusions drawn from the stress relaxation results that the HFZ hydrogels exhibited slower dynamics than the HFx hydrogels (Table 2). Note that τ_{max} for the HF30 sample did not fall on the same line in Figure 7c as did the HF10, HF20, and HFZ hydrogels. This may be a consequence of the much

DOI: 10.1021/acs.macromol.9b00830
Macromolecules 2019, 52, 6055−6067

lower water content in the HF30 sample and was not considered significant.

The series of rheological measurements demonstrate the unique combination of properties for the HFZ hydrogel, which are attractive for the potential applications of these tough hydrogels. These properties of the HFZ hydrogel appear to be associated with the cooperativity requirements for rearrangements that correspond with the relaxation processes of the two different physical cross-link mechanisms that are present on a single terpolymer chain. The statistical (random) incorporation of these functional groups on the chain appears to lead to distinct differences from block copolymers with similar functionality with increased sensitivity to the ionic cross-link units at lower Zn^{2+} concentrations.

■ CONCLUSIONS

The inclusion of an associating ionic group containing stoichiometric quantities of Zn^{2+} in an amphiphilic copolymer leads to substantial alteration of the mechanical properties of the resulting hydrogels. Unlike hydrogel with only hydrophobic cross-links, the addition of the ionic cross-links (HFZ hydrogel) enables hydrogels with both high elastic modulus and high swelling ratio. The ionic cross-links hindered the rearrangement of hydrophobic cross-links to dramatically increase the relaxation times of the HFZ hydrogel. These hydrogels can effectively self-heal their microstructure after damage caused by large strains. These results provide new insights into the mechanisms associated with dual physical cross-linked hydrogels in terms of their design through the manipulation of the relaxation time spectra through associations.

■ ASSOCIATED CONTENT

Supporting Information

The Supporting Information is available free of charge on the ACS Publications website at DOI: 10.1021/acs.macromol.9b00830.

^{1}H NMR spectra and SANS patterns of HEA/FOSM and HEA/FOSM/ZnA hydrogels; and fits of the stress relaxation response of HEA/FOSM and HEA/FOSM/ZnA hydrogels by generalized Maxwell model (PDF)

■ AUTHOR INFORMATION

Corresponding Authors

*E-mail: rweiss@uakron.edu (R.A.W.).
*E-mail: vogt@uakron.edu, bdv5051@psu.edu (B.D.V.).

ORCID

Chao Wang: 0000-0002-5205-9771
Nicole S. Zacharia: 0000-0001-7925-1416
R. A. Weiss: 0000-0002-5700-6871
Bryan D. Vogt: 0000-0003-1916-7145

Present Addresses

§Department of Chemical and Biomolecular Engineering, University of Delaware, Newark, Delaware 19716, United States (C.W.).
∥Department of Secondary Education, College of Education, Slippery Rock University, 1 Morrow Way, Slippery Rock, Pennsylvania 16057, United States (K.D.).

Author Contributions

The manuscript was written through contributions of all authors. All authors have given approval to the final version of the manuscript.

Funding

This work was financially supported by NSF-DMR #1659531 (NSF-REU program) and the Chemical, Bioengineering, Environmental and Transport Systems (CBET) Division in the Directorate for Engineering of the National Science Foundation under grant CBET-1606685.

Notes

The authors declare no competing financial interest.

■ ACKNOWLEDGMENTS

The research used the Complex Materials Scattering (CMS/11-BM) beamline, operated by the National Synchrotron Light Source II and the Center for Functional Nanomaterials, which are U.S. Department of Energy (DOE) Office of Science User Facilities operated for the DOE Office of Science by Brookhaven National Laboratory under Contract No. DE-SC0012704. Access to the NGB 30 m SANS was provided by the Center for High Resolution Neutron Scattering, a partnership between the National Institute of Standards and Technology and the National Science Foundation under Agreement No. DMR-1508249. The authors acknowledge the support of the National Institute of Standards and Technology, U.S. Department of Commerce, in providing the neutron research facilities used in this work. The authors thank Drs. Yimin Mao, Masafumi Fukuto, Ruipeng Li, and Yanfeng Xia for their help with scattering measurements.

■ REFERENCES

(1) Nowak, A. P.; Breedveld, V.; Pakstis, L.; Ozbas, B.; Pine, D. J.; Pochan, D.; Deming, T. J. Rapidly recovering hydrogel scaffolds from self-assembling diblock copolypeptide amphiphiles. *Nature* **2002**, *417*, 424.

(2) Suh, J. K. F.; Matthew, H. W. T. Application of chitosan-based polysaccharide biomaterials in cartilage tissue engineering: a review. *Biomaterials* **2000**, *21*, 2589−2598.

(3) Lee, K. Y.; Mooney, D. J. Hydrogels for tissue engineering. *Chem. Rev.* **2001**, *101*, 1869−1880.

(4) Costa, A. M. S.; Mano, J. F. Extremely strong and tough hydrogels as prospective candidates for tissue repair - A review. *Eur. Polym. J.* **2015**, *72*, 344−364.

(5) Gong, J. P.; Katsuyama, Y.; Kurokawa, T.; Osada, Y. Double-network hydrogels with extremely high mechanical strength. *Adv. Mater.* **2003**, *15*, 1155−1158.

(6) Shams Es-haghi, S.; Leonov, A. I.; Weiss, R. A. Deconstructing the double-network hydrogels: The importance of grafted chains for achieving toughness. *Macromolecules* **2014**, *47*, 4769−4777.

(7) Webber, R. E.; Creton, C.; Brown, H. R.; Gong, J. P. Large strain hysteresis and mullins effect of tough double-network hydrogels. *Macromolecules* **2007**, *40*, 2919−2927.

(8) Liang, S.; Wu, J.; Tian, H.; Zhang, L.; Xu, J. High-Strength Cellulose/Poly(ethylene glycol) Gels. *ChemSusChem* **2008**, *1*, 558−563.

(9) Zhang, J.; Wang, N.; Liu, W.; Zhao, X.; Lu, W. Intermolecular hydrogen bonding strategy to fabricate mechanically strong hydrogels with high elasticity and fatigue resistance. *Soft Matter* **2013**, *9*, 6331−6337.

(10) Hu, X.; Vatankhah-Varnoosfaderani, M.; Zhou, J.; Li, Q.; Sheiko, S. S. Weak Hydrogen Bonding Enables Hard, Strong, Tough, and Elastic Hydrogels. *Adv. Mater.* **2015**, *27*, 6899.

(11) Hunt, J. N.; Feldman, K. E.; Lynd, N. A.; Deek, J.; Campos, L. M.; Spruell, J. M.; Hernandez, B. M.; Kramer, E. J.; Hawker, C. J.

DOI: 10.1021/acs.macromol.9b00830
Macromolecules 2019, 52, 6055−6067

Tunable, High Modulus Hydrogels Driven by Ionic Coacervation. *Adv. Mater.* **2011**, *23*, 2327−2331.
(12) Sun, J.-Y.; Zhao, X.; Illeperuma, W. R. K.; Chaudhuri, O.; Oh, K. H.; Mooney, D. J.; Vlassak, J. J.; Suo, Z. Highly stretchable and tough hydrogels. *Nature* **2012**, *489*, 133−136.
(13) Li, J.; Illeperuma, W. B. K.; Suo, Z.; Vlassak, J. J. Hybrid Hydrogels with Extremely High Stiffness and Toughness. *ACS Macro Lett.* **2014**, *3*, 520−523.
(14) Luo, F.; Sun, T. L.; Nakajima, T.; Kurokawa, T.; Zhao, Y.; Sato, K.; Bin Ihsan, A.; Li, X.; Guo, H.; Gong, J. P. Oppositely Charged Polyelectrolytes Form Tough, Self-Healing, and Rebuildable Hydrogels. *Adv. Mater.* **2015**, *27*, 2722−2727.
(15) Abdurrahmanoglu, S.; Can, V.; Okay, O. Design of high-toughness polyacrylamide hydrogels by hydrophobic modification. *Polymer* **2009**, *50*, 5449−5455.
(16) Tuncaboylu, D. C.; Sari, M.; Oppermann, W.; Okay, O. Tough and self-healing hydrogels formed via hydrophobic interactions. *Macromolecules* **2011**, *44*, 4997−5005.
(17) Li, W.; An, H.; Tan, Y.; Lu, C.; Liu, C.; Li, P.; Xu, K.; Wang, P. Hydrophobically associated hydrogels based on acrylamide and anionic surface active monomer with high mechanical strength. *Soft Matter* **2012**, *8*, 5078−5086.
(18) Hao, J.; Weiss, R. A. Viscoelastic and mechanical behavior of hydrophobically modified hydrogels. *Macromolecules* **2011**, *44*, 9390−9398.
(19) Zhao, X. Multi-scale multi-mechanism design of tough hydrogels: building dissipation into stretchy networks. *Soft Matter* **2014**, *10*, 672−687.
(20) Zhao, X.; Huebsch, N.; Mooney, D. J.; Suo, Z. Stress-relaxation behavior in gels with ionic and covalent crosslinks. *J. Appl. Phys.* **2010**, *107*, No. 063509.
(21) Long, R.; Mayumi, K.; Creton, C.; Narita, T.; Hui, C.-Y. Time dependent behavior of a dual cross-link self-healing gel: Theory and experiments. *Macromolecules* **2014**, *47*, 7243−7250.
(22) Lin, D. C.; Douglas, J. F.; Horkay, F. Development of minimal models of the elastic properties of flexible and stiff polymer networks with permanent and thermoreversible cross-links. *Soft Matter* **2010**, *6*, 3548−3561.
(23) Zhang, H.; Peng, H.; Li, Y.; Xu, Y.; Weng, W. Compositional- and time-dependent dissipation, recovery and fracture toughness in hydrophobically reinforced hybrid hydrogels. *Polymer* **2015**, *80*, 130−137.
(24) Hao, J.; Weiss, R. A. Mechanical behavior of hybrid hydrogels composed of a physical and a chemical network. *Polymer* **2013**, *54*, 2174−2182.
(25) Sayil, C.; Okay, O. Macroporous poly(N-isopropyl) acrylamide networks: formation conditions. *Polymer* **2001**, *42*, 7639−7652.
(26) Zhang, H. J.; Sun, T. L.; Zhang, A. K.; Ikura, Y.; Nakajima, T.; Nonoyama, T.; Kurokawa, T.; Ito, O.; Ishitobi, H.; Gong, J. P. Tough Physical Double-Network Hydrogels Based on Amphiphilic Triblock Copolymers. *Adv. Mater.* **2016**, *28*, 4884−4890.
(27) Wang, X.-H.; Song, F.; Qian, D.; He, Y.-D.; Nie, W.-C.; Wang, X.-L.; Wang, Y.-Z. Strong and tough fully physically crosslinked double network hydrogels with tunable mechanics and high self-healing performance. *Chem. Eng. J.* **2018**, *349*, 588−594.
(28) Wei, D.; Yang, J.; Zhu, L.; Chen, F.; Tang, Z.; Qin, G.; Chen, Q. Fully physical double network hydrogels with high strength, rapid self-recovery and self-healing performances. *Polym. Test.* **2018**, *69*, 167−174.
(29) Jia, H.; Huang, Z.; Fei, Z.; Dyson, P. J.; Zheng, Z.; Wang, X. Unconventional tough double-network hydrogels with rapid mechanical recovery, self-healing, and self-gluing properties. *ACS Appl. Mater. Interfaces* **2016**, *8*, 31339−31347.
(30) Bastings, M. M. C.; Koudstaal, S.; Kieltyka, R. E.; Nakano, Y.; Pape, A. C. H.; Feyen, D. A. M.; Van Slochteren, F. J.; Doevendans, P. A.; Sluijter, J. P. G.; Meijer, E. W.; et al. A fast pH-switchable and self-healing supramolecular hydrogel carrier for guided, local catheter injection in the infarcted myocardium. *Adv. Healthcare Mater.* **2014**, *3*, 70−78.
(31) Zhang, H.; Xia, H.; Zhao, Y. Poly(vinyl alcohol) hydrogel can autonomously self-heal. *ACS Macro Lett.* **2012**, *1*, 1233−1236.
(32) Schäfer, S.; Kickelbick, G. Double Reversible Networks: Improvement of Self-Healing in Hybrid Materials via Combination of Diels−Alder Cross-Linking and Hydrogen Bonds. *Macromolecules* **2018**, 6099.
(33) Henderson, K. J.; Zhou, T. C.; Otim, K. J.; Shull, K. R. Ionically Cross-Linked Triblock Copolymer Hydrogels with High Strength. *Macromolecules* **2010**, *43*, 6193−6201.
(34) Tian, J.; Seery, T. A. P.; Ho, D. L.; Weiss, R. A. Physically cross-linked alkylacrylamide hydrogels: A SANS analysis of the microstructure. *Macromolecules* **2004**, *37*, 10001−10008.
(35) Wang, C.; Wiener, C. G.; Cheng, Z. W.; Vogt, B. D.; Weiss, R. A. Modulation of the Mechanical Properties of Hydrophobically Modified Supramolecular Hydrogels by Surfactant-Driven Structural Rearrangement. *Macromolecules* **2016**, *49*, 9228−9238.
(36) Wang, C.; Wiener, C. G.; Yang, Y. M.; Weiss, R. A.; Vogt, B. D. Structural rearrangement and stiffening of hydrophobically modified supramolecular hydrogels during thermal annealing. *J. Polym. Sci., Part B: Polym. Phys.* **2017**, *55*, 1036−1044.
(37) Wiener, C. G.; Wang, C.; Liu, Y.; Weiss, R. A.; Vogt, B. D. Nanostructure Evolution during Relaxation from a Large Step Strain in a Supramolecular Copolymer-Based Hydrogel: A SANS Investigation. *Macromolecules* **2017**, *50*, 1672−1680.
(38) Cohen, Y.; Ramon, O.; Kopelman, I. J.; Mizrahi, S. Characterization of inhomogeneous polyacrylamide hydrogels. *J. Polym. Sci., Part B: Polym. Phys.* **1992**, *30*, 1055−1067.
(39) Wang, F.; Weiss, R. A. Thermoresponsive Supramolecular Hydrogels with High Fracture Toughness. *Macromolecules* **2018**, *51*, 7386−7395.
(40) Wang, C.; Wiener, C. G.; Fukuto, M.; Li, R. P.; Yager, K. G.; Weiss, R. A.; Vogt, B. D. Strain rate dependent nanostructure of hydrogels with reversible hydrophobic associations during uniaxial extension. *Soft Matter* **2019**, *15*, 227−236.
(41) Li, X. F.; Zhao, Y. J.; Li, D. P.; Zhang, G. W.; Long, S. J.; Wang, H. Hybrid dual crosslinked polyacrylic acid hydrogels with ultrahigh mechanical strength, toughness and self-healing properties via soaking salt solution. *Polymer* **2017**, *121*, 55−63.
(42) Gustafson, R. L.; Lirio, J. A. Binding of divalent metal ions by crosslinked polyacrylic acid. *J. Phys. Chem. A* **1968**, *72*, 1502−1505.
(43) Porasso, R. D.; Benegas, J. C.; van den Hoop, M. Chemical and electrostatic association of various metal ions by poly(acrylic acid) and poly(methacrylic acid) as studied by potentiometry. *J. Phys. Chem. B* **1999**, *103*, 2361−2365.
(44) Yang, C. H.; Wang, M. X.; Haider, H.; Yang, J. H.; Sun, J. Y.; Chen, Y. M.; Zhou, J. X.; Suo, Z. G. Strengthening Alginate/Polyacrylamide Hydrogels Using Various Multivalent Cations. *ACS Appl. Mater. Interfaces* **2013**, *5*, 10418−10422.
(45) Horkay, F.; Tasaki, I.; Basser, P. J. Effect of monovalent-divalent cation exchange on the swelling of polyacrylate hydrogels in physiological salt solutions. *Biomacromolecules* **2001**, *2*, 195−199.
(46) Krzywon, J. *Demountable Titanium Cells*; NIST Center for Neutron Research, 2016; Vol. *2016*.
(47) Wang, C.; Wiener, C. G.; Sepulveda-Medina, P. I.; Ye, C. H.; Simmons, D. S.; Li, R. P.; Fukuto, M.; Weiss, R. A.; Vogt, B. D. Antifreeze Hydrogels from Amphiphilic Statistical Copolymers. *Chem. Mater.* **2019**, *31*, 135−145.
(48) Kline, S. R. Reduction and analysis of SANS and USANS data using IGOR Pro. *J. Appl. Crystallogr.* **2006**, *39*, 895−900.
(49) Ilavsky, J. Nika: software for two-dimensional data reduction. *J. Appl. Crystallogr.* **2012**, *45*, 324−328.
(50) Beaucage, G. Approximations leading to a unified exponential power-law approach to small-angle scattering. *J. Appl. Crystallogr.* **1995**, *28*, 717−728.
(51) Beaucage, G.; Schaefer, D. W. Structural studies of complex systems using small-angle scattering: a unified Guinier/power-law approach. *J. Non-Cryst. Solids* **1994**, *172*−*174*, 797−805.

DOI: 10.1021/acs.macromol.9b00830
Macromolecules 2019, 52, 6055−6067

(52) Ilavsky, J.; Jemian, P. R. Irena: tool suite for modeling and analysis of small-angle scattering. *J. Appl. Crystallogr.* **2009**, *42*, 347−353.
(53) Mark, J. E.; Erman, B. *Rubberlike Elasticity: A Molecular Primer*; Cambridge University Press, 2007.
(54) Tian, J.; Seery, T. A. P.; Weiss, R. A. Physically cross-linked alkylacrylamide hydrogels: Phase behavior and microstructure. *Macromolecules* **2004**, *37*, 9994−10000.
(55) Orakdogen, N.; Okay, O. Correlation between crosslinking efficiency and spatial inhomogeneity in poly (acrylamide) hydrogels. *Polym. Bull.* **2006**, *57*, 631−641.
(56) Luo, Y. D.; Montarnal, D.; Treat, N. J.; Hustad, P. D.; Christianson, M. D.; Kramer, E. J.; Fredrickson, G. H.; Hawker, C. J. Enhanced Block Copolymer Phase Separation Using Click Chemistry and Ionic Junctions. *ACS Macro Lett.* **2015**, *4*, 1332−1336.
(57) Bergman, R.; Swenson, J. Dynamics of supercooled water in confined geometry. *Nature* **2000**, *403*, 283−286.
(58) Pykal, M.; Langer, M.; Prudilova, B. B.; Banas, P.; Otyepka, M. Ion Interactions across Graphene in Electrolyte Aqueous Solutions. *J. Phys. Chem. C* **2019**, *123*, 9799−9806.
(59) Murakami, T.; Kawamori, T.; Gopez, J. D.; McGrath, A. J.; Klinger, D.; Saito, K. Synthesis of PEO-based physical gels with tunable viscoelastic properties. *J. Polym. Sci., Part A: Polym. Chem.* **2018**, *56*, 1033−1038.
(60) Jeong, K. J.; Panitch, A. Interplay between Covalent and Physical Interactions within Environment Sensitive Hydrogels. *Biomacromolecules* **2009**, *10*, 1090−1099.
(61) Varghese, S.; Lele, A. K.; Srinivas, D.; Mashelkar, R. A. Role of hydrophobicity on structure of polymer-metal complexes. *J. Phys. Chem. B* **2001**, *105*, 5368−5373.
(62) Baumgaertel, M.; Winter, H. H. Determination of discrete relaxation and retardation time spectra from dynamic mechanical data. *Rheol. Acta* **1989**, *28*, 511−519.
(63) Phadke, A.; Zhang, C.; Arman, B.; Hsu, C. C.; Mashelkar, R. A.; Lele, A. K.; Tauber, M. J.; Arya, G.; Varghese, S. Rapid self-healing hydrogels. *Proc. Natl. Acad. Sci. U.S.A.* **2012**, *109*, 4383−4388.
(64) Hayward, R. C.; Pochan, D. J. Tailored Assemblies of Block Copolymers in Solution: It Is All about the Process. *Macromolecules* **2010**, *43*, 3577−3584.
(65) Semenov, B. N. On Conditions of Modelling and Choice of Viscoelastic Coatings for Drag Reduction. In *Recent Developments in Turbulence Management*; Choi, K. S., Ed.; Springer, 1991; pp 241−262.

DOI: 10.1021/acs.macromol.9b00830
Macromolecules 2019, 52, 6055−6067